PHYSICAL REVIEW B **109**, 165435 (2024)

Stable phases of freestanding monolayer TiO_2: Emergence of out-of-plane ferroelectricity

Xiangtian Bu,[1] Haitao Liu,[2,3] and Yuanchang Li[1,*]
[1]*Key Lab of Advanced Optoelectronic Quantum Architecture and Measurement (MOE), and Advanced Research Institute of Multidisciplinary Science, Beijing Institute of Technology, Beijing 100081, China*
[2]*Institute of Applied Physics and Computational Mathematics, Beijing 100088, China*
[3]*National Key Laboratory of Computational Physics, Beijing 100088, China*

(Received 5 February 2024; revised 26 March 2024; accepted 12 April 2024; published 23 April 2024)

Despite being successfully synthesized [Zhang *et al.*, Nat. Mater. **20**, 1073 (2021)], the monolayer structure of stable hexagonal TiO_2 is unknown, and it is not even clear whether it can exist in a freestanding form. Through first-principles calculations, we have identified two previously uncharted stable structures, namely, distorted $1 \times \sqrt{3}$ $1T$-TiO_2 and $\sqrt{3} \times \sqrt{3}$ $1T$-TiO_2, both of which are energetically more favorable than commonly adopted $1H$ and $1T$ phases. Here, structural distortions are characterized by the out-of-plane shifts of Ti atoms due to the pseudo-Jahn-Teller interactions, which break one and all two inversion symmetries of $1T$ configuration. As a consequence, the $1 \times \sqrt{3}$ $1T$ remains centrosymmetric, while the $\sqrt{3} \times \sqrt{3}$ $1T$ exhibits out-of-plane ferroelectricity. Electronic structure calculations show that both are wide-band-gap semiconductors with band gaps larger than their bulk counterparts. In this paper, we not only deepen the understanding of structural instability in wide-gap semiconductors but also add a member to the rare family of two-dimensional out-of-plane ferroelectrics.

DOI: 10.1103/PhysRevB.109.165435

I. INTRODUCTION

Titanium dioxide (TiO_2) has long been recognized as one of the most promising photocatalysts for the production of hydrogen from water using solar energy [1]. Its application, however, has been hampered by a wide band gap of >3 eV, which limits it to absorbing only the ultraviolet portion of the solar spectrum. As this fraction accounts for only ~5% of the solar radiation on Earth, efforts have been made to narrow the band gap of TiO_2 to utilize a wider range of the solar spectrum and improve the conversion efficiency. Current band gap optimization strategies focus on introducing midgap states through doping [2–6], but this has proven to be difficult. Two-dimensional TiO_2 offers an alternative as its dopant-free phase has been found to have a narrow band gap ~2.1 eV [7]. Recently, a planar hexagonal TiO_2 monolayer was synthesized by strictly controlled oxidation at the metal-gas interface with a band gap of 2.35 eV [8], which is almost optimal for visible light absorption. However, its unknown crystal structure constrains the understanding of the band gap reduction.

Generally, the band gap of layered materials increases as the number of layers decreases due to quantum size effects. For nonlayered materials, such as III-V semiconductors, one does find a band gap decrease for monolayers, but the crystal structure changes significantly compared with the bulk phase [9–11]. Regarding the hexagonal TiO_2 monolayer, it is still not even clear whether it can be stabilized in a freestanding form. Although the $1H$-TiO_2 band gap calculated using the Heyd-Scuseria-Ernzerhof functional agrees with the experimental results [8], this alone is not sufficient to determine the structure because of the well-known fact that the band gap of transition-metal oxides from DFT-based approaches depends strongly on the exchange-correlation functionals used [12–15]. In terms of formation energy, $1H$-TiO_2 is 0.36 (0.53) eV/atom higher than $1T$-TiO_2 by the PBE (PBE + U) calculation [13,14], suggesting difficulty in synthesizing it at thermal equilibrium. More importantly, both $1H$- and $1T$-TiO_2 are unstable with imaginary frequencies on their phonon spectra [12]. It has been reported that the imaginary frequencies of $1T$-TiO_2 can be eliminated when considering Hubbard U [13]. Nevertheless, this elimination depends on the size of U, and there is no universal U that reproduces the crystal and electronic structure as well as the phase stability of TiO_2 at the same time [16]. Historically, a stable structure known as Lepidocrocite type has been proposed [17], but its out-of-plane O-Ti-O-O-Ti-O layer order renders it more like a bilayer. In addition, the Ti atoms therein form a tetragonal rather than a hexagonal lattice.

In this paper, we perform extensive first-principles calculations on the structural and electronic properties of a hexagonal TiO_2 monolayer and identify two stable configurations, namely, distorted $1 \times \sqrt{3}$ $1T$-TiO_2 and $\sqrt{3} \times \sqrt{3}$ $1T$-TiO_2 (denoted hereafter as $d1T$ and $t1T$, respectively, depending on the number of Ti atoms in the unit cell). This distortion manifests itself as an out-of-plane shift of Ti, which on the one hand reduces the system energy and eliminates imaginary frequencies, thus stabilizing the structure. On the other hand, it breaks one and all two spatial inversion symmetries of $1T$ to form $d1T$ and $t1T$, respectively. As a result, the motions of the two Ti atoms in $d1T$ are always centrosymmetric, whereas in $t1T$, the

---

[*] yuancli@bit.edu.cn

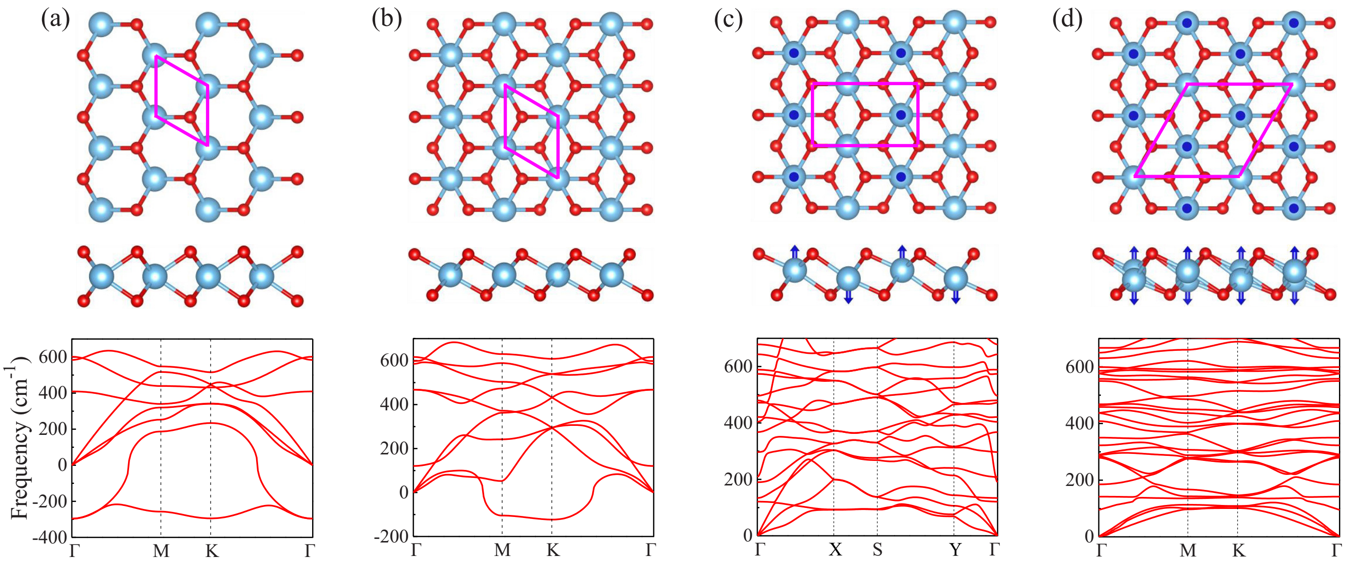

FIG. 1. Geometric structures and phonon spectra of monolayer TiO_2 with configurations of (a) $1H$, (b) $1T$, (c) $d1T$, and (d) $t1T$. First and second rows correspond to top and side views, respectively. Pink rectangles denote the unit cells, and cyan and red balls denote Ti and O atoms. In (c) and (d), blue arrows mark the Ti displacements relative to their positions in the $1T$ configuration.

inversion symmetry is spontaneously broken, giving rise to an inherent out-of-plane ferroelectricity of 0.5 μC/cm^2. Unlike in transition-metal dichalcogenides where ferroelectricity appears across the metal-insulator transition [18,19], $1T$-TiO_2 is a wide-gap semiconductor whose structural instability is driven by the pseudo-Jahn-Teller mechanism [20]. Electronic structure calculations show that band gaps of both $d1T$ and $t1T$ are larger than that of bulk TiO_2, hinting at an important influence of the substrate on the experimentally observed band gap narrowing [8]. In this paper, we not only deepen the understanding of structural instability in wide-gap semiconductors but also add a member to the rare family of two-dimensional out-of-plane ferroelectrics.

II. METHODOLOGY AND MODELS

All density functional theory (DFT) calculations were performed within the formalism of the Perdew-Burke-Ernzerhof (PBE) [21] exchange-correlation functional as implemented in VASP[22]. The projector augmented-wave method [23] was employed with an energy cutoff of 520 eV. A vacuum layer of 18 Å was used to minimize spurious interactions between adjacent images. Integration over the Brillouin zone was done using the Monkhorst-Pack k-point grids of $24 \times 24 \times 1$, $24 \times 15 \times 1$, $18 \times 18 \times 1$, and $8 \times 8 \times 12$ for $1H/1T$, $d1T$, $t1T$ monolayer, and bulk rutile. The lattice constants and atomic positions were fully optimized until the residual force on each atom was <1 meV/Å. The van der Waals interaction was included using Grimme's D2 scheme [24], which is considered necessary to reproduce the fact that the bulk rutile is lower in energy than the anatase [8,13]. Quasiparticle G_0W_0 calculations [25] were performed to fix the band gap problem of PBE, with the number of empty bands exceeding 6 times the valence bands. Optical gaps and exciton spectra were obtained by solving the Bethe-Salpeter equation (BSE) [26] on top of the G_0W_0 results. Ferroelectric polarization was calculated using the Berry-phase method [27]. The phonon spectra were calculated within density functional perturbation theory using the QUANTUM ESPRESSO package [28], with the cutoff energy of 80 Ry, the same k-point grids as above, and the q-point grids of $8 \times 8 \times 1$, $8 \times 5 \times 1$, and $6 \times 6 \times 1$ for $1H/1T$, $d1T$, and $t1T$.

III. RESULTS AND DISCUSSION

Honeycomblike $1H$ and $1T$ structures are common in monolayers of transition-metal oxides and dichalcogenides. However, both $1H$- and $1T$-TiO_2 are unstable, as evidenced by the imaginary frequencies on their phonon spectra [see Figs. 1(a) and 1(b)]. The presence of a soft phonon band throughout the Brillouin zone means that $1H$ is unlikely to exist in a freestanding form. In contrast, the soft phonon modes of $1T$ are predominantly present on the MK line, which can usually be eliminated by enlarging the cell and allowing relative motion between otherwise equivalent atoms.

When relaxation starts from slightly deviating perfect $1 \times \sqrt{3}$ $1T$ and $\sqrt{3} \times \sqrt{3}$ $1T$ supercells, we obtain the stable structures $d1T$ and $t1T$, as shown in Figs. 1(c) and 1(d), respectively. Both no longer have soft phonon modes. The energy of $d1T$ is 19 meV/Ti lower than that of $1T$, while the energy of $t1T$ is further reduced by 7 meV/Ti. Note that, in d^2 transition-metal dichalcogenides such as MoS_2, different phases ($2H$, $1T$, and $1T'$) are experimentally observed [29,30], even though their energy differences are an order of magnitude larger than here [31]. It is therefore reasonable to speculate that both $d1T$ and $t1T$ could potentially be prepared experimentally.

We are aware that bulk TiO_2 has a variety of phases whose relative stability depends on the different exchange-correlation functionals used in the calculations [16]. For this reason, we have performed HSE06 and PBE + U calculations. HSE06 is consistent with PBE in that both predict structural distortions. Specifically, the energy of $d1T$ is 8 meV/Ti lower than that of $1T$, while the energy of $t1T$ is

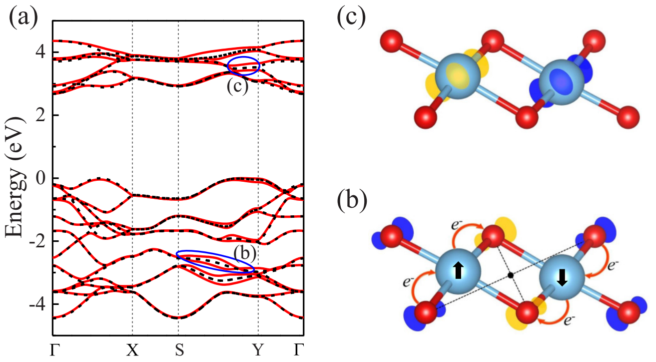

FIG. 2. (a) Comparison between the PBE band structures of 1T (black dashed lines) and second intermediate (red solid lines). The valence band maximum is set as energy zero. (b) [(c)] Charge density difference between the two splitting O-p (Ti-d) bands with an isosurface of 0.3 (0.1) $e/\text{Å}^3$. The electron accumulation and depletion regions are depicted in yellow and blue, respectively. In (b), the red arrows illustrate the electron donation from the O atom on one side to the empty Ti-d orbitals and then back-donation to the O atom on the other side. This drives the Ti atom out of plane in the direction denoted by black arrows and makes it no longer the center of inversion. However, this does not destroy the other inversion center indicated by the black dot, so $d1T$ is still centrosymmetric.

further reduced by 7 meV/Ti. For comparison, the PBE + U results show a dependence on the value of U. Increasing U tends to suppress the distortion by decreasing the energy gain of the structural distortion. At U = 3 eV, the structural distortion disappears completely. Previous studies on bulk TiO_2 [16] have shown that there is no universal U that can simultaneously provide the correct cell parameters, relative phase stability, and electronic gap. Furthermore, around U = 3 eV, PBE + U fails to predict the structural instability of $TiSe_2$ [32]. In contrast, HSE06 reproduces well the cell parameters and electronic gap of bulk TiO_2 as well as the structural instability of $TiSe_2$. However, it fails to reproduce the relative stability of rutile and anatase TiO_2. Although more experimental evidence is needed to test whether nonlocal exchange or on-site electron-electron interactions dominate in TiO_2, there is no doubt that its hexagonal monolayer is indeed capable of existing in the freestanding form.

Here, $d1T$ and $t1T$ essentially maintain the in-plane hexagonal skeleton, with the most pronounced deformation being the out-of-plane shifts of the Ti atoms. Specifically, the two Ti in $d1T$ are symmetrically shifted upward and downward by 0.19 and −0.19 Å, respectively, and consequently, it still has inversion symmetry. On the contrary, one of the three Ti atoms in $t1T$ is shifted upward by 0.28 Å, while the remaining two are shifted downward by 0.14 Å. Such asymmetric shifts break spatial inversion symmetry and produce a separation of positive and negative charge centers. As a result, $t1T$ shows a spontaneous polarization of 0.5 $\mu\text{C/cm}^2$ along the out-of-plane direction but zero in-plane polarization. The polarization strength is ∼1.4 times that in MoS_2 [18,33]. The presence of out-of-plane ferroelectricity would lead to a kink in the corresponding potential energy profile [34], which is indeed the case here. The shift of Ti changes the Ti-O bonds from a uniform 1.98 Å in 1T to 1.87–2.12 Å in $d1T$ or $t1T$, with the Ti-Ti spacing narrowing or elongating by 0.02–0.07 Å.

For applications, out-of-plane ferroelectricity is more advantageous than in-plane ferroelectricity, yet out-of-plane ferroelectricity tends to disappear below a critical thickness due to depolarizing field effects [35]. In contrast, in-plane polarization is insensitive to thickness and remains stable at the atomic thickness limit [36]. Out-of-plane ferroelectricity was theoretically predicted in monolayer MoS_2 [18] and experimentally verified later in $MoTe_2$ [37]. Interestingly, similar distorted $1 \times \sqrt{3}$ and $\sqrt{3} \times \sqrt{3}$ structures exist for $MoS_2/MoTe_2$, also the former centrosymmetric and the latter ferroelectric [19]. In view of this, a comparison with them helps to deepen the understanding of structural instability and ferroelectricity observed here.

Under the 1T configuration, the local D_{3d} field splits the metal 3d orbitals into a lower-lying t_{2g} triplet and a higher-lying e_g doublet. For the Mo of group 6, after crystallization into $MoS_2/MoTe_2$, the two remaining d electrons can only partially occupy the t_{2g} triplet. This triggers the Jahn-Teller instability, leading to a further splitting of the t_{2g} triplet, accompanied by a metal-insulator transition. Differently, Ti belongs to group 4, so the characteristic electronic configuration of TiO_2 is always d^0, regardless of its crystal structure. Therefore, its 3d occupancy must be empty, with the result that each configuration of TiO_2 has a band gap separating the O-2p from theTi-3d states. This is evidenced by our first-principles calculations shown later.

Hence, there must be another mechanism driving the deformation of 1T-TiO_2. One possibility is excitonic insulators, i.e., lattice distortion is triggered when electrons and holes at different k points in the Brillouin zone spontaneously form excitons due to Coulomb attraction [38–41]. While this mechanism has traditionally been introduced for semimetals with small band overlaps or semiconductors with small band gaps, in recent years, it has been found that the excitonic instability may also play a role in atomic-thick monolayers with one-electron gaps >3 eV [40,41]. To this end, we have calculated the exciton spectrum of 1T using YAMBO code [42] and found a minimum exciton formation energy of ∼3 eV, thus ruling out the excitonic insulator mechanism.

To understand the structural distortions here, we insert four intermediate structures uniformly between 1T and $d1T$. Figure 2(a) compares the bands of 1T and the second intermediate [43], which reveals that the Ti displacement lifts the degeneracy of the occupied O-p bands and the unoccupied Ti-d bands along the SY line. This hints at an interaction between the O-p and Ti-d bands and is a signal of the pseudo-Jahn-Teller effect [20,44]. In Figs. 2(b) and 2(c), we representatively plot the charge density difference between the two splitting occupied and unoccupied bands circled in blue. In Fig. 2(b), the pseudo-Jahn-Teller interaction leads to a charge redistribution between the upper- and lower-layer O atoms connected to the same Ti, causing them to be no longer equivalent. This breaks the inversion symmetry with respect to the Ti atoms. Bader analysis shows that the O atoms in the blue (yellow) regions of Fig. 2(b) lose (gain) a small number of electrons. Combining the above facts, we can build a picture of the structural distortion due to the pseudo-Jahn-Teller interaction. It triggers a charge transfer in which electrons are donated from one

TABLE I. Summarization of the space group, the minimum gaps calculated by different methods, and optical gap ($E_{\rm opt}$, defined as the first peak on the imaginary part of the calculated dielectric function) of various two-dimensional TiO_2 monolayers. The bulk rutile is taken for a comparison.

		Minimum gap (eV)			
TiO_2	Space group	PBE	HSE06	G_0W_0	$E_{\rm opt}$ (eV)
$t1T$	$P31m$	2.92	4.52	5.38	3.99
$d1T$	$P2_1/m$	2.85	4.45	5.36	4.21
$1T$	$P\bar{3}m1$	2.67	4.12	5.09	3.68
$1H$	$P\bar{6}m2$	1.18	2.61	3.74	3.69
Rutile	$P4_2/mnm$	1.82	3.32	3.22	3.94

O atom to the empty Ti d orbitals and then back-donated to another O atom, as depicted by the red arrows in Fig. 2(b). This donation–back-donation drives the central Ti atom to move vertically in the direction of charge transfer, reducing the system energy while inducing structural distortions. However, we note that the other inversion center of $1T$ [black dot in Fig. 2(b)] is preserved under the pseudo-Jahn-Teller interaction. Its existence forces the two Ti atoms to move symmetrically up and down, corresponding to the split higher and lower conduction bands [see Fig. 2(c)]. The case of $t1T$ is quite different because there is no center of symmetry between the three Ti. Thus, their disproportionate movements in the out-of-plane direction lead to spontaneous polarization.

We further consider the phonon softening condition of the pseudo-Jahn-Teller theory [44]:

$$\langle\Delta\rangle < \frac{8F^2}{K_0}. \tag{1}$$

The $\langle\Delta\rangle$ is half of the energy gap between the mixing electronic states, which is derived directly from the band structure of $1T$. The F and K_0 are the vibronic coupling constant and the primary force constant, respectively, which can be fitted from the energetic calculations of the DFT. Within the pseudo-Jahn-Teller theory, the adiabatic potential energy surface $U(Q)$ is expressed as a function of the structural displacement Q ($Q^2 = Q_x^2 + Q_y^2 + Q_z^2$):

$$U(Q) = \frac{1}{2}K_0Q^2 - 2\sum_{a=x,y,z}\left[\sqrt{\Delta^2 + 2F^2\left(Q^2 - Q_a^2\right)}\right]. \tag{2}$$

Take, for example, the calculation of the K point where phonon softening occurs (see Fig. 1). From the band structure of $1T$, we have $\langle\Delta\rangle = 1.97$ eV. Then using DFT total energies of $1T$, the second intermediate, $d1T$, and their Q displacements with respect to $1T$, we get $F = 1.7$ eV/Å, $K_0 = 11$ eV/Å^2, and $8F^2/K_0 = 2.1$ eV. Unambiguously, Eq. (1) is satisfied, justifying that it is indeed the pseudo-Jahn-Teller mechanism at work.

Next, we turn to the electronic properties. Since PBE severely underestimates the band gap of bulk TiO_2, we carry out different levels of calculations. Rutile TiO_2, which is the most stable bulk phase, is used for comparison. Some of the characteristic results are listed in Table I, and the typical band structures of $d1T$ and $t1T$ are plotted in Fig. 3. Rutile TiO_2 has a PBE band gap of 1.82 eV and an optical band gap of 3.94 eV, which are in agreement with previous studies [45]. Although the calculated band gaps are method dependent, both the fundamental and optical band gaps of $d1T$ and $t1T$ are significantly larger than those of rutile under the same method. In fact, the fundamental band gap obtained by each method for $1T$ is also larger than that of rutile. Nevertheless, the PBE and HSE06 band gaps of $1H$ are smaller than that of rutile. Comparison of these monolayer results reveals a tendency for the fundamental band gap to increase as the system energy decreases.

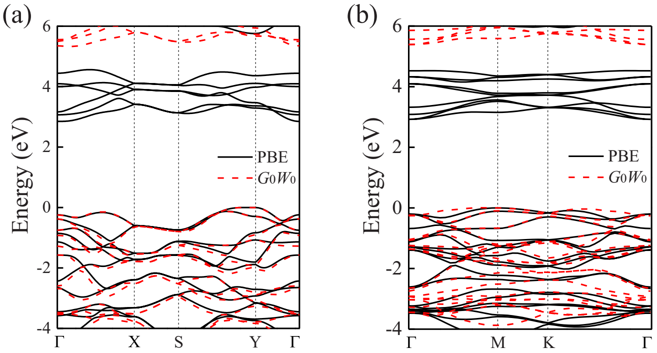

FIG. 3. Band structures of (a) $d1T$-TiO_2 and (b) $t1T$-TiO_2, respectively, calculated by PBE and G_0W_0. The valence band maximum is set as energy zero.

Our preceding structural calculations indicate that the freestanding TiO_2 monolayer does exist. Whether it is $1T$, $d1T$, or $t1T$, it matches the experimentally observed planar honeycomblike hexagonal crystal structure and the measured thickness [8]. However, as far as the band gap is concerned, our comparisons at the same level consistently support the fact that the band gap of the monolayer is larger, not smaller, than that of the bulk. One aspect of the band gap discrepancy may arise from first-principles calculations. It is well known that there is no method that ensures reproducing the correct band gap. Even the method that reproduces the bulk TiO_2 band gap is not guaranteed to yield the correct band gap for the monolayer. On the other hand, the experimental conditions are different from first-principles simulations in terms of temperature, substrate, and sample (e.g., defects). All these may lead to variations in the band gap.

Here, we briefly discuss some experimental possibilities. One is the strain effect of the substrate used in the experiment, which does reduce the band gap. For example, a 5% in-plane strain shrinks the PBE band gap of $d1T$ and $t1T$ by ∼5% and 11%, to 2.72 and 2.60 eV, respectively. From this estimation, a strain of at least 17% is required to make the fundamental band gap smaller than that of the bulk, which sounds difficult. Nonetheless, their optical band gaps of 3.80 and 3.60 eV do become smaller than the bulk rutile.

Another possibility is the presence of $1H$ due to temperature-enhanced stability, which has relatively small band gaps (see Table I). To calculate the effect of temperature on the phonon spectrum, we vary the Fermi-Dirac distribution function that describes the probability of occupation of the electronic states by varying the smearing parameter. By this means, we can assess the structural stability at different temperatures [46]. It was found that the soft phonon modes of both $1H$ and $1T$ gradually harden as the smearing increases. At a smearing of 0.8 eV, there are no more soft modes on the phonon spectrum (not shown). Although smearing does not directly correspond to the temperature, such dependence suggests that $1H$ and $1T$ can stabilize at sufficiently high temperatures. However, on the other hand, our energetic calculations show that the relative stability trend of $d1T > 1T > 1H$ remains unchanged even in the presence of strain ($\leqslant \pm 5\%$) or electronic doping ($\leqslant 2.5 \times 10^{14}/\mathrm{cm}^2$). These point to a crucial role of kinetic factors and/or entropic effects in the experimental observations.

IV. CONCLUSIONS

In summary, by first-principles calculations, we predict stable hexagonal monolayers of $d1T$-TiO$_2$ and $t1T$-TiO$_2$, the latter of which is particularly intriguing because of its intrinsic out-of-plane ferroelectricity. It is the d^0 nature of Ti that distinguishes the physics associated with structural distortion here from the widely studied d^2 dichalcogenides. First, it occurs in a wide-gap semiconductor with the absence of a metal-insulator transition. Second, it is driven by a pseudo-Jahn-Teller effect involving interactions with excited states. Third, it is characterized by out-of-plane motions of metal atoms instead of in-plane dimerization and trimerization. These results provide useful insights into the understanding of the recent experiment. On the other hand, it is interesting to note that the d^0 and d^2 systems exhibit the commonality of both having two distorted $1T$ structures, one of which remains centrosymmetric, while the other is ferroelectric. Whether this is a commonality dictated by the two centers of symmetry of the $1T$ structures is worth exploring in the future.

ACKNOWLEDGMENTS

This paper was supported by the Ministry of Science and Technology of China (Grants No. 2023YFA1406400 and No. 2020YFA0308800) and the National Natural Science Foundation of China (Grants No. 12074034 and No.11874089).

---

[1] A. Fujishima and K. Honda, Electrochemical photolysis of water at a semiconductor electrode, Nature (London) **238**, 37 (1972).

[2] R. Asahi, T. Morikawa, T. Ohwaki, K. Aoki, and Y. Taga, Visible-light photocatalysis in nitrogen-doped titanium oxides, Science **293**, 269 (2001).

[3] Y. Gai, J. Li, S. S. Li, J. B. Xia, and S. H. Wei, Design of narrow-gap TiO$_2$: A passivated codoping approach for enhanced photoelectrochemical activity, Phys. Rev. Lett. **102**, 036402 (2009).

[4] W. Zhu, X. Qiu, V. Iancu, X. Q. Chen, H. Pan, W. Wang, N. M. Dimitrijevic, T. Rajh, H. M. Meyer, III, M. P. Paranthaman *et al.*, Band gap narrowing of titanium oxide semiconductors by noncompensated anion-cation codoping for enhanced visible-light photoactivity, Phys. Rev. Lett. **103**, 226401 (2009).

[5] W.-J. Yin, S.-H. Wei, M. M. Al-Jassim, and Y. Yan, Double-hole-mediated coupling of dopants and its impact on band gap engineering in TiO$_2$, Phys. Rev. Lett. **106**, 066801 (2011).

[6] P. Wang, Z. Liu, F. Lin, G. Zhou, J. Wu, W. Duan, B.-L. Gu, and S. B. Zhang, Optimizing photoelectrochemical properties of TiO$_2$ by chemical codoping, Phys. Rev. B **82**, 193103 (2010).

[7] J. Tao, T. Luttrell, and M. Batzill, A two-dimensional phase of TiO$_2$ with a reduced bandgap, Nat. Chem. **3**, 296 (2011).

[8] B. Y. Zhang, K. Xu, Q. F. Yao, A. Jannat, G. H. Ren, M. R. Field, X. M. Wen, C. H. Zhou, A. Zavabeti, and J. Z. Ou, Hexagonal metal oxide monolayers derived from the metal-gas interface, Nat. Mater. **20**, 1073 (2021).

[9] Z. Y. Jiang, Y. C. Li, S. B. Zhang, and W. H. Duan, Realizing an intrinsic excitonic insulator by decoupling exciton binding energy from the minimum band gap, Phys. Rev. B **98**, 081408(R) (2018).

[10] S. Dong and Y. C. Li, Excitonic instability and electronic properties of AlSb in the two-dimensional limit, Phys. Rev. B **104**, 085133 (2021).

[11] L. Qin, Z. H. Zhang, Z. Y. Jiang, K. Fan, W. H. Zhang, Q. Y. Tang, H. N. Xia, F. Q. Meng, Q. H. Zhang, L. Gu *et al.*, Realization of AlSb in the double-layer honeycomb structure: A robust class of two-dimensional material, ACS Nano **15**, 8184 (2021).

[12] C. Ataca, H. Şahin, and S. Ciraci, Stable, single-layer MX$_2$ transition-metal oxides and dichalcogenides in a honeycomb-like structure, J. Phys. Chem. C **116**, 8983 (2012).

[13] I. Kim, G. Lee, and M. Choi, First-principles investigation of two-dimensional $1T$-TiO$_2$, Phys. Rev. Mater. **4**, 094001 (2020).

[14] F. A. Rasmussen and K. S. Thygesen, Computational 2D materials database: Electronic structure of transition-metal dichalcogenides and oxides, J. Phys. Chem. C **119**, 13169 (2015).

[15] H. Tan, H. Liu, Y. Li, W. Duan, and S. Zhang, Understanding the origin of bandgap problem in transition and post-transition metal oxides, J. Chem. Phys. **151**, 124703 (2019).

[16] M. E. Arroyo-de Dompablo, A. Morales-García, and M. Taravillo, DFT+U calculations of crystal lattice, electronic structure, and phase stability under pressure of TiO$_2$ polymorphs, J. Chem. Phys. **135**, 054503 (2011).

[17] H. Sato, K. Ono, T. Sasaki, and A. Yamagishi, First-principles study of two-dimensional titanium dioxides, J. Phys. Chem. B **107**, 9824 (2003).

[18] S. N. Shirodkar and U. V. Waghmare, Emergence of ferroelectricity at a metal-semiconductor transition in a $1T$ monolayer of MoS$_2$, Phys. Rev. Lett. **112**, 157601 (2014).

[19] E. Bruyer, D. Di Sante, P. Barone, A. Stroppa, M.-H. Whangbo, and S. Picozzi, Possibility of combining ferroelectricity and Rashba-like spin splitting in monolayers of the $1T$-type transition-metal dichalcogenides MX_2 ($M =$ Mo, W; $X =$ S, Se, Te), Phys. Rev. B **94**, 195402 (2016).

[20] V. Z. Polinger, P. Garcia-Fernandez, and I. B. Bersuker, Pseudo Jahn-Teller origin of ferroelectric instability in BaTiO$_3$ type perovskites: The Green's function approach and beyond, Phys. B: Condens. Matter **457**, 296 (2015).

[21] J. P. Perdew, K. Burke, and M. Ernzerhof, Generalized gradient approximation made simple, Phys. Rev. Lett. **77**, 3865 (1996).

[22] G. Kresse and J. Furthmüller, Efficient iterative schemes for *ab initio* total-energy calculations using a plane-wave basis set, Phys. Rev. B **54**, 11169 (1996).

[23] P. E. Blöchl, Projector augmented-wave method, Phys. Rev. B **50**, 17953 (1994); G. Kresse and D. Joubert, From ultrasoft pseudopotentials to the projector augmented-wave method, *ibid.* **59**, 1758 (1999).

[24] S. Grimme, Semiempirical GGA-type density functional constructed with a long-range dispersion correction, J. Comput. Chem. **27**, 1787 (2006).

[25] M. S. Hybertsen and S. G. Louie, Electron correlation in semiconductors and insulators: Band gaps and quasiparticle energies, Phys. Rev. B **34**, 5390 (1986).

[26] M. Rohlfing and S. G. Louie, Electron-hole excitations and optical spectra from first principles, Phys. Rev. B **62**, 4927 (2000).

[27] R. D. King-Smith and D. Vanderbilt, Theory of polarization of crystalline solids, Phys. Rev. B **47**, 1651 (1993).

[28] P. Giannozzi, O. Andreussi, T. Brumme, O. Bunau, M. B. Nardelli, M. Calandra, R. Car, C. Cavazzoni, D. Ceresoli, M. Cococcioni *et al.*, Advanced capabilities for materials modelling with QUANTUM ESPRESSO, J. Phys.: Condens. Matter **29**, 465901 (2017).

[29] R. Kappera, D. Voiry, S. Yalcin, B. Branch, G. Gupta, A. D. Mohite, and M. Chhowalla, Phase-engineered low-resistance contacts for ultrathin MoS_2 transistors, Nat. Mater. **13**, 1128 (2014).

[30] L. Liu, J. Wu, L. Wu, M. Ye, X. Liu, Q. Wang, S. Hou, P. Lu, L. Sun, J. Zheng *et al.*, Phase-selective synthesis of $1T'$ MoS_2 monolayers and heterophase bilayers, Nat. Mater. **17**, 1108 (2018).

[31] K. N. Duerloo, Y. Li, and E. J. Reed, Structural phase transitions in two-dimensional Mo- and W-dichalcogenide monolayers, Nat. Commun. **5**, 4214 (2014).

[32] M. Hellgren, J. Baima, R. Bianco, M. Calandra, F. Mauri, and L. Wirtz, Critical role of the exchange interaction for the electronic structure and charge-density-wave formation in $TiSe_2$, Phys. Rev. Lett. **119**, 176401 (2017).

[33] Since the bulk TiO_2 has a nonlayered structure, we calculate the polarization strength here using the thickness of a monolayer, i.e., 3 and 2 Å for MoS_2 and $t1T$-TiO_2, respectively. Thus, the result of 0.36 $\mu C/cm^2$ differs from 0.18 $\mu C/cm^2$ in Ref. [18].

[34] Z. J. Wang and Z. R. Liu, Novel piezoelectricity in two-dimensional metallic/semimetallic materials with out-of-plane polarization, J. Phys. Chem. Lett. **14**, 7549 (2023).

[35] J. Shang, X. Tang, and L. Kou, Two dimensional ferroelectrics: Candidate for controllable physical and chemical applications, Wiley Interdiscip, Rev. Comput. Mol. Sci. **11**, e1496 (2021).

[36] K. Chang, J. W. Liu, H. C. Lin, N. Wang, K. Zhao, A. M. Zhang, F. Jin, Y. Zhong, X. P. Hu, W. H. Duan *et al.*, Discovery of robust in-plane ferroelectricity in atomic-thick SnTe, Science **353**, 274 (2016).

[37] S. Yuan, X. Luo, H. L. Chan, C. Xiao, Y. Dai, M. Xie, and J. Hao, Room-temperature ferroelectricity in $MoTe_2$ down to the atomic monolayer limit, Nat. Commun. **10**, 1775 (2019).

[38] D. Jérome, T. M. Rice, and W. Kohn, Excitonic insulator, Phys. Rev. **158**, 462 (1967).

[39] A. Kogar, S. Vig, M. S. Rak, A. A. Husain, F. Flicker, Y. I. Joe, L. Venema, G. J. MacDougall, T. C. Chiang, E. Fradkin *et al.*, Signatures of exciton condensation in a transition metal dichalcogenide, Science **358**, 1314 (2017).

[40] Z. Jiang, Y. Li, W. Duan, and S. Zhang, Half-excitonic insulator: A single-spin Bose-Einstein condensate, Phys. Rev. Lett. **122**, 236402 (2019).

[41] Z. Y. Jiang, W. K. Lou, Y. Liu, Y. C. Li, H. F. Song, K. Chang, W. H. Duan, and S. B. Zhang, Spin-triplet excitonic insulator: The case of semihydrogenated graphene, Phys. Rev. Lett. **124**, 166401 (2020).

[42] D. Sangalli, A. Ferretti, H. Miranda, C. Attaccalite, I. Marri, E. Cannuccia, P. Melo, M. Marsili, F. Paleari, A. Marrazzo *et al.*, Many-body perturbation theory calculations using the YAMBO code, J. Phys.: Condens. Matter **31**, 325902 (2019).

[43] Here, physics does not depend on which intermediate is chosen, just for clarity.

[44] I. B. Bersuker, Jahn-Teller and Pseudo-Jahn-Teller effects: From particular features to general tools in exploring molecular and solid state properties, Chem. Rev. **121**, 1463 (2021).

[45] T. Zhu and S.-P. Gao, The stability, electronic structure and optical property of TiO_2 polymorphs, J. Phys. Chem. C **118**, 11385 (2014).

[46] N. D. Mermin, Thermal properties of the inhomogeneous electron gas, Phys. Rev. **137**, A1441 (1965).